



MOX-Report No. 60/2020

**Hierarchical model reduction driven by a Proper
Orthogonal Decomposition for parametrized
advection-diffusion-reaction problems**

Lupo Pasini, M; Perotto, S.

MOX, Dipartimento di Matematica
Politecnico di Milano, Via Bonardi 9 - 20133 Milano (Italy)

mox-dmat@polimi.it

<http://mox.polimi.it>

Hierarchical model reduction driven by a Proper Orthogonal Decomposition for parametrized advection-diffusion-reaction problems

Massimiliano Lupo Pasini[‡], Simona Perotto*

August 18, 2020

*MOX– Dipartimento di Matematica, Politecnico di Milano
Piazza L. da Vinci 32, I-20133 Milano, Italy

[‡] Computational Sciences and Engineering Division, Oak Ridge National Laboratory
1 Bethel Valley Road, Oak Ridge, TN, USA, 37831
lupopasini@ornl.gov, simona.perotto@polimi.it

Abstract

This work combines the Hierarchical Model (HiMod) reduction technique with a standard Proper Orthogonal Decomposition (POD) to solve parametrized partial differential equations modeling advection-diffusion-reaction phenomena in elongated domains (e.g., pipes). This combination leads to what we define a HiPOD model reduction, which merges the reliability of HiMod with the computational efficiency of POD. Two different HiPOD techniques are presented and assessed through an extensive numerical verification.

This manuscript has been authored in part by UT-Battelle, LLC, under contract DE-AC05-00OR22725 with the US Department of Energy (DOE). The US government retains and the publisher, by accepting the article for publication, acknowledges that the US government retains a nonexclusive, paid-up, irrevocable, worldwide license to publish or reproduce the published form of this manuscript, or allow others to do so, for US government purposes. DOE will provide public access to these results of federally sponsored research in accordance with the DOE Public Access Plan (<http://energy.gov/downloads/doe-public-access-plan>).

1 Motivations

Parametrized partial differential equations (PDEs) arise in several contexts such as inverse problems, control, optimization, uncertainty quantification, and risk assessment. In most of these applications, the number of parameters may become very large, so that an efficient numerical approximation of parametric PDEs represents a challenging computational issue (see, e.g., [2, 6, 7, 3]). Parametric model order reduction aims

at reducing the computational effort associated with a parametric modeling in many-query and real-time tasks, where the occurrence of the curse of dimensionality raises the necessity to propose numerical methods to sustain the computational cost.

Many of the model reduction techniques currently employed in engineering practice exploit the offline/online paradigm to efficiently reduce the numerical effort. This is the case, for instance, of the well-known reduced basis method [17, 33], where, during the offline phase, a reduced basis is precomputed by solving a high-fidelity model (the “truth”) for certain samples of the parameter, while, in the online phase, the reduced model is evaluated to predict a new scenario (i.e., for a value of the parameter not previously sampled). From a practical viewpoint, the offline stage remains the bottleneck of an offline/online decomposition, especially when many samples are needed like for multiparametric problems.

To tackle this issue, we propose to replace the “truth” with a reduced order model which exhibits a high accuracy although characterized by a contained computational demand. For this purpose, we employ the reduced solution provided by a Hierarchical Model (HiMod) discretization [12, 28, 31, 26] as high fidelity model. HiMod reduction proved to be an effective tool to model partial differential problems characterized by a privileged dynamics aligned with the dominant direction of the domain (e.g., flows of fluid in channels, pipes or vessels), which may be locally modified by secondary dynamics evolving along the transverse sections of the tube [29, 15, 8]. Analogously to other model reduction procedures [34, 9, 16, 14, 10, 24], a HiMod discretization moves from a standard separation of variables and approximates the mainstream and the secondary dynamics by means of different numerical methods. For instance, in the seminal papers, the main direction of the flux is discretized by one-dimensional (1D) finite elements, while the transverse dynamics are recovered by using few degrees of freedom, via a suitable modal basis. This separate discretization yields a system of coupled 1D problems, whose coefficients include the effect of the transverse dynamics. The reliability exhibited by HiMod is considerably higher compared with standard 1D reduced models, whereas the computational effort remains absolutely affordable. Indeed, HiMod reduction is characterized by a linear dependence of the computational cost on the number of degrees of freedom in contrast to a standard finite element model which demands a suitable power of such a number. The reduced basis is generated by using a data-driven procedure. Following [4], we resort to a standard Proper Orthogonal Decomposition (POD) [21, 22, 20, 19, 36]. This choice allows us to set what we define as a HiPOD model reduction. On the one hand, the employment of the HiMod discretization significantly reduces the computational effort of the offline phase without compromising its reliability; on the other hand, the online phase relies on the efficiency of a POD formulation, so that a system of very small dimensionality is solved to approximate the parametric problem at hand.

In this paper, we focus on two HiPOD model reduction procedures. The first approach is very straightforward and it has been introduced in [4]. The second variant, which represents the actual novelty of the paper, is more complex and takes advantage of the separation of variables implied by a HiMod discretization. We also attempt a

comparison between the HiPOD approaches, despite the heterogeneity of the two procedures.

The paper is organized as follows. Section 2 applies the HiMod discretization to a reference parametric advection-diffusion-reaction problem and numerically assesses the reliability of the high-fidelity model. Section 3 introduces the two HiPOD model reduction procedures, and provides an extensive numerical verification to investigate the robustness of the proposed approaches with respect to the truncation of the POD basis, the extrapolation, and the possibility to explore multi-parametric settings. Finally, some conclusions are drawn in the last section, and possible future developments of the current work are provided.

2 HiMod reduction: the basic

HiMod reduction is performed under the specific assumption that the computational domain, $\Omega \subset \mathbb{R}^d$ with $d = 2, 3$, can be expressed as a Cartesian product, $\bigcup_{x \in \Omega_{1D}} \{x\} \times \Sigma_x$, where Ω_{1D} is a 1D horizontal supporting fiber, while $\Sigma_x \subset \mathbb{R}^{d-1}$ denotes the transverse section at the generic point x along Ω_{1D} [12, 28, 31, 26]. The reference geometry is a pipe, where the dominant dynamic is parallel to Ω_{1D} , whereas the transverse dynamics occur along fibers Σ_x . For the sake of simplicity, we select $\Omega_{1D} \equiv (a, b) \subset \mathbb{R}$. For the general case where Ω_{1D} coincides with a bent centerline, we refer to [25, 29, 8]. Then, via an invertible map $\Psi : \Omega \rightarrow \hat{\Omega}$, we change the physical domain Ω into a reference domain $\hat{\Omega} = \Omega_{1D} \times \hat{\Sigma}$, which shares the same supporting fiber as in Ω , and where $\hat{\Sigma} \subset \mathbb{R}^{d-1}$ denotes the reference fiber. In particular, for any point $\mathbf{z} = (x, \mathbf{y}) \in \Omega$, there exists a point $\hat{\mathbf{z}} = (\hat{x}, \hat{\mathbf{y}}) \in \hat{\Omega}$, such that $\hat{\mathbf{z}} = \Psi(\mathbf{z})$, with $\hat{x} \equiv x$ and $\hat{\mathbf{y}} = \psi_x(\mathbf{y})$, where $\psi_x : \Sigma_x \rightarrow \hat{\Sigma}$ is the map between the generic and the reference transverse fiber. Hereafter, we assume ψ_x to be a C^1 -diffeomorphism for all $x \in \Omega_{1D}$, and Ψ to be differentiable with respect to \mathbf{z} . The reference domain $\hat{\Omega}$ represents the setting where the computations are actually performed, and where all the constants can be explicitly computed. More details about maps Ψ and ψ_x are available in [28].

As a reference problem, we choose a parametrized elliptic PDE, defined on Ω , which can be recast into the following weak form: given the parameter $\alpha \in \mathcal{P}$,

$$\text{find } u(\alpha) \in V \quad \text{s.t.} \quad a(u(\alpha), v; \alpha) = f(v; \alpha) \quad \forall v \in V, \quad (1)$$

where $\mathcal{P} \subset \mathbb{R}^p$ is the set of the admissible parameters; $V \subseteq H^1(\Omega)$ is a Hilbert space depending on the PDE problem and on the selected boundary conditions, with standard notation for function spaces [11]; $a(\cdot, \cdot; \alpha) : V \times V \times \mathcal{P} \rightarrow \mathbb{R}$ and $f(\cdot; \alpha) : V \times \mathcal{P} \rightarrow \mathbb{R}$ denote a parametrized bilinear and linear form, respectively, where the linearity property holds with respect to all the variables but α . Suitable hypotheses are imposed on the problem data to guarantee the well-posedness of formulation (1), for any $\alpha \in \mathcal{P}$. Moreover, we assume an affine parameter dependence [17, 33].

We focus on a scalar linear advection-diffusion-reaction (ADR) problem completed, for the sake of simplicity, with full homogeneous Dirichlet boundary conditions, so that

the bilinear and the linear forms in (1) are

$$a(w, z; \alpha) = \int_{\Omega} \mu \nabla w \cdot \nabla z \, d\Omega + \int_{\Omega} (\mathbf{b} \cdot \nabla w + \sigma w) z \, d\Omega, \quad f(z; \alpha) = \int_{\Omega} f z \, d\Omega, \quad (2)$$

with $w, z \in V = H_0^1(\Omega)$. The parameter α coincides with one or several of the problem data, chosen among the viscosity μ , the advective field $\mathbf{b} = [b_1, \dots, b_d]^T$, the reaction coefficient σ , the source term f , or a boundary value when boundary conditions, more general with respect to the homogeneous Dirichlet data, are assigned.

HiMod reduction performs a different discretization along the supporting and the transverse directions. For this purpose, we introduce a 1D discrete space, $V_{1D} \subset H_0^1(\Omega_{1D})$ with $\dim(V_{1D}) = N_h < +\infty$, of functions vanishing at a and b , and a modal basis $\{\varphi_k\}_{k \in \mathbb{N}^+}$ of functions defined on $\widehat{\Sigma}$ which are orthonormal with respect to the $L^2(\widehat{\Sigma})$ -scalar product and which satisfy the data assigned on $\Gamma_L = \cup_{x \in \Omega_{1D}} \partial \Sigma_x$. For further details about the choice of the modal basis, also in the presence of general boundary data on Γ_L , we refer to [1, 15, 28]. Concerning V_{1D} , a standard choice is the finite element space [12, 28, 31, 26, 30, 32] or an isogeometric discretization when Ω is not rectilinear [29, 8]. Thus, the HiMod reduced space can be defined as

$$V_m = \left\{ v_m(x, \mathbf{y}; \alpha) = \sum_{k=1}^m \sum_{j=1}^{N_h} \tilde{v}_{k,j}^\alpha \vartheta_j(x) \varphi_k(\psi_x(\mathbf{y})), \text{ for } x \in \Omega_{1D}, \mathbf{y} \in \Sigma_x, \alpha \in \mathcal{P} \right\},$$

with $\{\vartheta_j\}_{j=1}^{N_h}$ a basis for the space V_{1D} , so that $\tilde{v}_k(x; \alpha) = \sum_{j=1}^{N_h} \tilde{v}_{k,j}^\alpha \vartheta_j(x) \in V_{1D}$ denotes the frequency coefficient of v_m associated with the k -th modal function φ_k .

The modal index $m \in \mathbb{N}^+$ establishes the level of detail of the HiMod approximation in the hierarchy, $\{V_m\}_m$, of reduced spaces. This index is selected by the user through some preliminary (geometric or physical) information about the problem at hand, or via an automatic procedure based on an a posteriori modeling error analysis [30, 32]. Additionally, index m can be the same in the whole Ω , or it can be locally tuned along the domain to match possible heterogeneities of the solution. We refer the interested reader to [31, 26], where a survey about the different criteria to choose m is provided.

The HiMod approximation to problem (1) becomes

$$\text{find } u_m(\alpha) = u_m(x, \mathbf{y}; \alpha) \in V_m \quad \text{s.t.} \quad a(u_m(\alpha), v_m; \alpha) = f(v_m; \alpha) \quad \forall v_m \in V_m, \quad (3)$$

for a given parameter $\alpha \in \mathcal{P}$ and for a selected modal index $m \in \mathbb{N}^+$. Following [28], we add a conformity and a spectral approximability assumption on the HiMod space, V_m , to ensure the well-posedness of formulation (3), along with a standard density assumption on space V_{1D} to guarantee the convergence of the HiMod approximation $u_m(\alpha)$ to the full solution $u(\alpha)$ in (1). From a computational viewpoint, after applying the HiMod expansion to the solution $u_m(\alpha)$ in (3) and choosing the test function v_m as the generic product $\vartheta_t \varphi_q$, with $q = 1, \dots, m$ and $t = 1, \dots, N_h$, the HiMod

formulation turns into the system

$$A_m(\alpha)\mathbf{u}_m(\alpha) = \mathbf{f}_m(\alpha), \quad (4)$$

of m 1D coupled problems, where $A_m(\alpha) \in \mathbb{R}^{mN_h \times mN_h}$ and $\mathbf{f}_m(\alpha) \in \mathbb{R}^{mN_h}$ are the HiMod stiffness matrix and right-hand side, while $\mathbf{u}_m(\alpha) \in \mathbb{R}^{mN_h}$ is the vector describing the solution,

$$u_m(x, \mathbf{y}; \alpha) = \sum_{k=1}^m \sum_{j=1}^{N_h} \tilde{u}_{k,j}^\alpha \vartheta_j(x) \varphi_k(\psi_x(\mathbf{y})), \quad (5)$$

discretized via the HiMod approach, where $\{\tilde{u}_{k,j}^\alpha\}_{k=1,j=1}^{m,N_h}$ are the modal coefficients (see [12, 28] for additional computational details).

When the mainstream dominates the transverse dynamics (i.e., for small values of m), the HiMod procedure has been shown to considerably reduce the computational burden associated with a standard discretization of problem (1), without affecting the accuracy of the simulation [23, 15, 8].

2.1 Reliability check of the HiMod reduction

The numerical assessment of this paper focuses on the two-dimensional (2D) setting. In this section, we qualitatively investigate the reliability of the HiMod reduction on two ADR problems completed with different boundary conditions, and we disregard the role played by the PDE parameters at this stage. For the HiMod discretization, we resort to linear finite elements (FE) along Ω_{1D} , whereas we describe the transverse dynamics with a sinusoidal modal basis. For a quantitative analysis as well as for a three-dimensional (3D) verification of the HiMod approximation, we refer the reader to [28, 1, 15, 8].

2.1.1 Test case 1

We define the domain Ω as the rectangle $(0, 3) \times (0, 1)$, while the problem data in (2) are

$$\mu(x, y) = 1, \quad \mathbf{b}(x, y) = [3, 0]^T, \quad \sigma(x, y) = 0, \quad f(x, y) = 1 - 2x + 3y. \quad (6)$$

The image at the top of Figure 1 shows the reference (full) solution computed with linear FE on a uniform unstructured grid of 260058 triangles. The chosen data justify the diffusive trend of the solution, which alternates a maximum to a minimum area.

With regards to the HiMod approximation, we subdivide the supporting fiber $[0, 3]$ into 60 uniform subintervals and we discretize the transverse dynamics by gradually increasing the number, m , of modal basis functions. The bottom panels in Figure 1 show the HiMod approximations for $m = 1$ (left) and $m = 2$ (right). It is evident that two modes are enough for ensuring a qualitatively good accuracy to the reduced solution, with a considerable reduction in terms of degrees of freedom (dofs) (120 dofs for the HiMod approximation to be compared with 373464 dofs for the FE model).

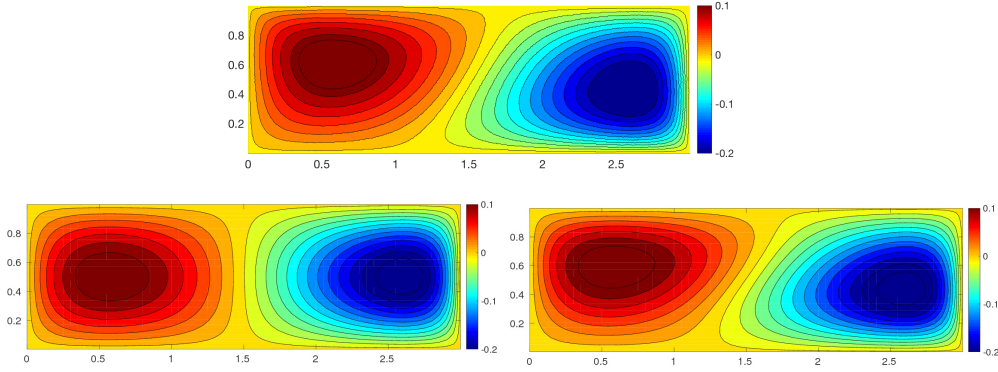


Figure 1: HiMod verification (test case 1): reference FE (top) and HiMod (bottom) solution for $m = 1$ (left) and $m = 2$ (right).

2.1.2 Test case 2

The domain Ω is now taken as the rectangle $(0, 6) \times (0, 1)$ and we select the problem data as

$$\begin{aligned} \mu(x, y) &= 0.24, \quad \mathbf{b}(x, y) = [5, \sin(6x)]^T, \quad \sigma(x, y) = 0, \\ f(x, y) &= 10\chi_{C_1}(x, y) + 10\chi_{C_2}(x, y), \end{aligned} \quad (7)$$

where χ_ω denotes the characteristic function associated with the generic region $\omega \subset \mathbb{R}^2$, while C_1 and C_2 identify the ellipsoidal areas $\{(x, y) : (x - 0.75)^2 + 0.4(y - 0.25)^2 < 0.01\}$ and $\{(x, y) : (x - 0.75)^2 + 0.4(y - 0.75)^2 < 0.01\}$, respectively. The ADR problem is completed with a homogeneous Neumann data on $\Gamma_N = \{(x, y) : x = 6, 0 \leq y \leq 1\}$ and by a homogeneous Dirichlet condition on $\Gamma_D = \partial\Omega \setminus \Gamma_N$, so that $V \equiv H_{\Gamma_D}^1(\Omega)$ in (1). The top image of Figure 2 displays the contour plot of the approximation obtained with linear FE on a uniform and unstructured mesh consisting of 553448 elements. We draw the attention of the reader to the oscillatory dynamics induced by the sinusoidal field, and the presence of the two localized sources in C_1 and C_2 . Notice that no stabilization is applied, despite the convection overcomes the diffusion. HiMod reduction is applied by introducing a uniform subdivision of Ω_{1D} into 120 subintervals and by employing an increasing number of modes. We do not introduce any stabilization also for the HiMod discretization. Figure 2, second-fourth row shows the HiMod approximation for $m = 2$, $m = 3$ and $m = 5$, respectively. At least five modes have to be employed to obtain a qualitatively reliable HiMod solution. As expected, the number of HiMod dofs is considerably lower compared with the FE case (600 versus 375296 dofs).

3 HiPOD techniques

The goal of the HiPOD techniques is to build a HiMod approximation for problem (1) at a computational cost lower with respect to the one characterizing the HiMod system

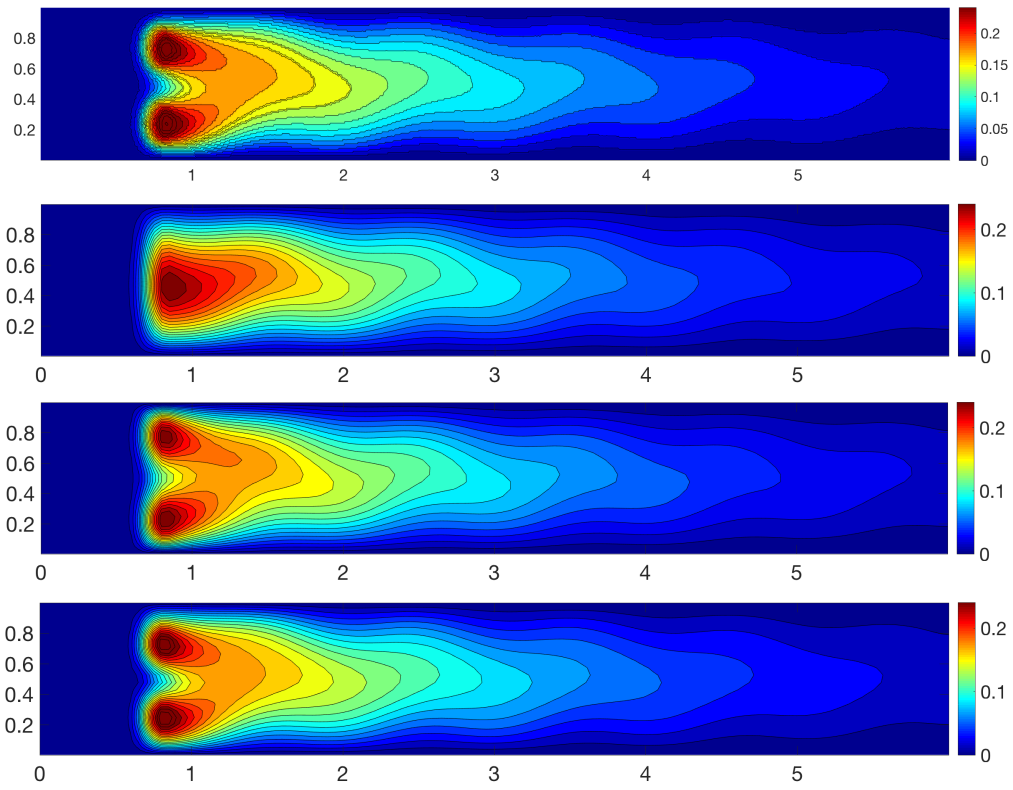


Figure 2: HiMod verification (test case 2): reference FE (first row) and HiMod solution for $m = 2$ (second row), $m = 3$ (third row) and $m = 5$ (fourth row).

(4). For this purpose, we resort to a POD approach, by adopting the offline/online paradigm [21, 22, 20, 19, 36]. In particular, during the offline phase, we discretize problem (1) via HiMod for different choices of α , to extract the POD (reduced) basis; in the online phase, we employ such a basis to approximate the HiMod solution to (1) for a value, $\alpha = \alpha^*$, of the parameter not yet sampled.

In this paper we explore two different HiPOD approaches. The first one is the most straightforward one, and resorts to a projection procedure to perform the online phase [4]. In the second approach, we drive the online phase by means of an interpolation procedure, following [37]. Moreover, this second variant somehow takes advantage of the separation of variables implied by a HiMod discretization. The leading feature of a HiPOD technique is to contain the computational burden typical of an offline phase. Actually, the POD is applied to solutions which have already been reduced via HiMod, in contrast to standard approaches where full solutions (e.g., finite element approximations) are employed to sample the phenomenon at hand. Notice that, a priori, any model reduction technique may replace the HiMod discretization during the offline phase.

3.1 The basic HiPOD approach

We start the *offline phase* by assembling the snapshot (or response) matrix S . To this aim, we select p different values, α_i , of the parameter α , and we compute the HiMod approximation to the associated problem (1), for $i = 1, \dots, p$. We employ the same discretization along Ω_{1D} and the same modal expansion for the transverse dynamics, so that, according to representation (5), each HiMod solution is identified by the mN_h coefficients $\{\tilde{u}_{k,j}^{\alpha_i}\}_{k=1,j=1}^{m,N_h}$ or, likewise, by vector

$$\mathbf{u}_m(\alpha_i) = \left[\underbrace{\tilde{u}_{1,1}^{\alpha_i}, \dots, \tilde{u}_{1,N_h}^{\alpha_i}}_{k=1}, \underbrace{\tilde{u}_{2,1}^{\alpha_i}, \dots, \tilde{u}_{2,N_h}^{\alpha_i}}_{k=2}, \dots, \underbrace{\tilde{u}_{m,1}^{\alpha_i}, \dots, \tilde{u}_{m,N_h}^{\alpha_i}}_{k=m} \right]^T \in \mathbb{R}^{mN_h}, \quad (8)$$

collecting the modal coefficients by mode. Thus, we assemble the snapshot matrix

$$S = [\mathbf{u}_m(\alpha_1), \mathbf{u}_m(\alpha_2), \dots, \mathbf{u}_m(\alpha_p)] \in \mathbb{R}^{(mN_h) \times p}, \quad (9)$$

and the matrix

$$\mathcal{V} = S - \frac{1}{p} \sum_{i=1}^p [\mathbf{u}_m(\alpha_i), \mathbf{u}_m(\alpha_i), \dots, \mathbf{u}_m(\alpha_i)] \in \mathbb{R}^{(mN_h) \times p}$$

characterized by a null average. Matrix \mathcal{V} is the array actually employed to extract the POD basis. For this purpose, we apply the Singular Value Decomposition (SVD) to \mathcal{V} , to obtain

$$\mathcal{V} = \Phi \Sigma \Psi^T, \quad (10)$$

where $\Phi \in \mathbb{R}^{(mN_h) \times (mN_h)}$ and $\Psi \in \mathbb{R}^{p \times p}$ are the unitary matrices gathering the left and the right singular vectors of \mathcal{V} , while $\Sigma = \text{diag}(\sigma_1, \dots, \sigma_\gamma) \in \mathbb{R}^{(mN_h) \times p}$ is the pseudo-diagonal matrix of the singular values of \mathcal{V} , with $\sigma_1 \geq \sigma_2 \geq \dots \geq \sigma_\gamma \geq 0$ and $\gamma = \min(mN_h, p)$ [13]. In the numerical assessment below, we always assume $\gamma = p$.

The decomposition (10) allows us to define the POD orthogonal reduced basis, being the set of the first l most significant left singular vectors, $\{\phi_i\}_{i=1}^l$, of \mathcal{V} , so that the reduced POD space is $V_{\text{POD}}^l = \text{span}\{\phi_1, \dots, \phi_l\}$, with $\dim(V_{\text{POD}}^l) = l$ and, in general, $l \ll mN_h$.

As to the choice of the integer l , different criteria can be adopted. For instance, one can analyze the trend of the spectrum Σ or introduce a control on the variance, by selecting the first l ordered singular values such that

$$R_l = \frac{\sum_{i=1}^l \sigma_i^2}{\sum_{i=1}^p \sigma_i^2} \geq \epsilon, \quad (11)$$

for a positive user-defined tolerance ϵ [36].

Remark 3.1 *As an alternative to the procedure above, the POD basis can be derived by applying the spectral decomposition to the covariance matrix $C = \mathcal{V}^T \mathcal{V} \in \mathbb{R}^{p \times p}$, being assumed $p \ll mN_h$. In particular, it holds that $\lambda_i = \sigma_i^2$, and $\phi_i = \lambda_i^{-1} S \mathbf{c}_i$, where $\{\lambda_i, \mathbf{c}_i\}$ denotes the generic {eigenvalue, eigenvector} pair associated with C , for $i = 1, \dots, p$ [36].*

Remark 3.2 (Snapshot choice) *The choice of representative values for the parameter α in (9) is a critical issue to make POD effective in practice. In general, it strictly depends on the problem at hand. In particular, the model reduction is effective if the selected snapshots cover the whole parameter space. This aspect is beyond the goal of this work, albeit extremely interesting.*

Now, the *online phase* approximates the HiMod solution to problem (1) for the value α^* of the parameter, with $\alpha^* \neq \alpha_i$ for $i = 1, \dots, p$, at a lower computational cost with respect to directly solving the HiMod system (4) for $\alpha = \alpha^*$. For this purpose, we project system (4) onto the POD space, V_{POD}^l , by computing the POD stiffness matrix and right-hand side,

$$A_{\text{POD}}(\alpha^*) = (\Phi_{\text{POD}}^l)^T A_m(\alpha^*) \Phi_{\text{POD}}^l \in \mathbb{R}^{l \times l}, \quad \mathbf{f}_{\text{POD}}(\alpha^*) = (\Phi_{\text{POD}}^l)^T \mathbf{f}_m(\alpha^*) \in \mathbb{R}^l, \quad (12)$$

respectively, where matrix $\Phi_{\text{POD}}^l = [\phi_1, \dots, \phi_l] \in \mathbb{R}^{(mN_h) \times l}$ collects the POD basis vectors by column, while $A_m(\alpha^*)$ and $\mathbf{f}_m(\alpha^*)$ are the HiMod stiffness matrix and right-hand side in (4). Then, we solve the POD system of order l

$$A_{\text{POD}}(\alpha^*) \mathbf{u}_{\text{POD}}(\alpha^*) = \mathbf{f}_{\text{POD}}(\alpha^*), \quad (13)$$

with $\mathbf{u}_{\text{POD}}(\alpha^*) = [u_{\text{POD},1}^{\alpha^*}, \dots, u_{\text{POD},l}^{\alpha^*}]^T \in \mathbb{R}^l$. This allows us to approximate the HiMod solution $\mathbf{u}_m(\alpha^*)$ in (4) by using the POD basis as

$$\mathbf{u}_m(\alpha^*) \approx \mathbf{u}_{\text{HiPOD}}^l(\alpha^*) = \sum_{s=1}^l u_{\text{POD},s}^{\alpha^*} \phi_s \in \mathbb{R}^{mN_h},$$

after solving a system of order l instead of mN_h . Finally, thanks to expansion (5), we obtain the HiPOD approximation $u_{\text{HiPOD}}^l(\alpha^*)$ to $u_m(x, \mathbf{y}; \alpha^*)$.

The assembly of $A_m(\alpha^*)$ and $\mathbf{f}_m(\alpha^*)$ in (12) constitutes the bottleneck of the basic HiPOD method, although this represents a computational burden typical of any projection-based POD procedure. Nevertheless, the employment of a reduced rather than a full model when building matrix S leads to a considerable reduction of the computational effort, especially when m is a small value.

3.1.1 Numerical assessment

The basic HiPOD procedure is assessed on the test problems in Section 2.1.

Test case 3

To perform the offline phase, we assume an affine dependence of the problem data in (2) on the independent variables, so that

$$\begin{aligned}\mu(\mathbf{x}) &= \mu_0 + \mu_x x + \mu_y y, & \mathbf{b}(\mathbf{x}) &= [b_0 + b_x x, b_1 + b_y y]^T, \\ \sigma(\mathbf{x}) &= \sigma_0 + \sigma_x x + \sigma_y y, & f(\mathbf{x}) &= f_0 + f_x x + f_y y.\end{aligned}$$

Then, we hierarchically reduce 30 different problems, by setting $\mu_0 = 1$, $\sigma_x = \sigma_y = 0$, $f_0 = 1$, and by randomly varying the remaining nine parameters as

$$\begin{aligned}\mu_x &\in \mathcal{P}_{\mu_x} = [0, 2], & \mu_y &\in \mathcal{P}_{\mu_y} = [0, 2], & \sigma_0 &\in \mathcal{P}_{\sigma_0} = [0, 3], \\ b_0 &\in \mathcal{P}_{b_0} = [0, 3], & b_1 &\in \mathcal{P}_{b_1} = [0, 3], & b_x &\in \mathcal{P}_{b_x} = [0, 2], \\ b_y &\in \mathcal{P}_{b_y} = [0, 2], & f_x &\in \mathcal{P}_{f_x} = [-2, 2], & f_y &\in \mathcal{P}_{f_y} = [-2, 2],\end{aligned}$$

so that the parameter in (1) coincides with the vector $\alpha = [\mu_x, \mu_y, \sigma_0, b_0, b_1, b_x, b_y, f_x, f_y]^T \in \mathbb{R}^9$ varying in $\mathcal{P} = \mathcal{P}_{\mu_x} \times \mathcal{P}_{\mu_y} \times \mathcal{P}_{\sigma_0} \times \mathcal{P}_{b_0} \times \mathcal{P}_{b_1} \times \mathcal{P}_{b_x} \times \mathcal{P}_{b_y} \times \mathcal{P}_{f_x} \times \mathcal{P}_{f_y}$.

The HiMod discretization uses linear FE along the mainstream, associated with a uniform partition of Ω_{1D} into 60 subintervals, and a modal expansion based on 10 sinusoidal modes. Figure 3, left shows the spectrum of matrix \mathcal{V} , where the vertical lines identify the dimension l for the POD space adopted in the online phase. The singular values decrease rather slowly until a drop occurs at $l = 17$ (being $\text{rank}(\mathcal{V})=17$). This can be ascribed to the large number of parameters involved, which limits the redundancy across the snapshots. During the online phase we approximate the same problem as in Section 2.1.1, so that

$$\alpha^* = [0, 0, 0, 3, 0, 0, 0, -2, 3]^T \in \mathcal{P},$$

and the reference HiMod solution is the one in Figure 1, bottom-right. Starting from the spectrum to the left side of Figure 3, we pick $l = 2, 4, 7, 15, 17$. The corresponding value for the ratio R_l in (11) is given by 0.9352, 0.9832, 0.9952, 0.9999, 1, respectively. Figure 4 provides the contour plots of $u_{\text{HiPOD}}^l(\alpha^*)$ for $l = 2, 7, 15$. Solutions

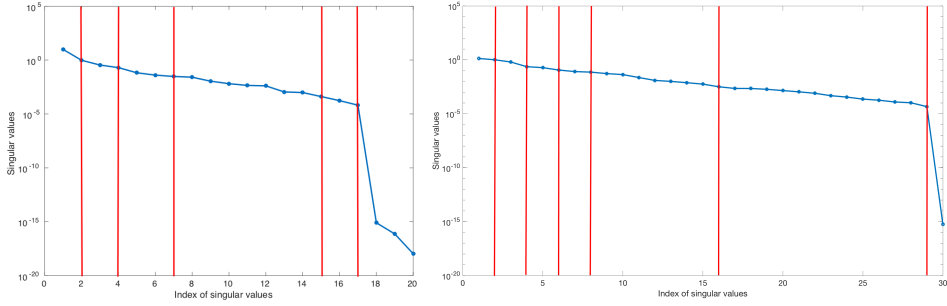


Figure 3: Basic HiPOD reduction: singular values of matrix \mathcal{V} for test case 3 (left) and 4 (right).

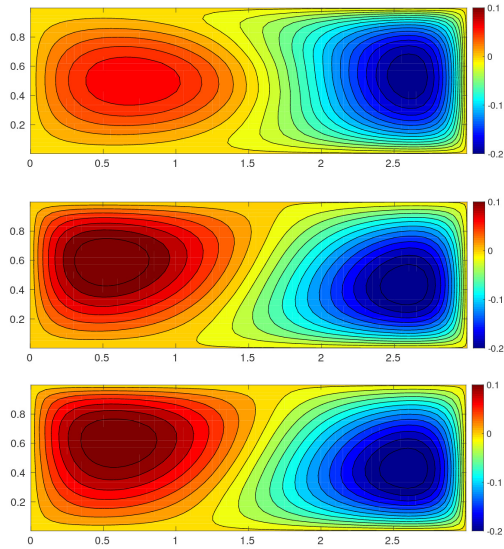


Figure 4: Basic HiPOD reduction (test case 3): HiPOD approximation for $l = 2$ (top), $l = 7$ (middle) and $l = 15$ (bottom).

$u_{\text{HiPOD}}^2(\boldsymbol{\alpha}^*)$ and $u_{\text{HiPOD}}^7(\boldsymbol{\alpha}^*)$ exhibit a good accuracy if we take into account that they are obtained by solving a system of dimensionality 2 and 7, respectively and that we are varying 9 parameters, contemporarily. The quality of the HiPOD approximation gradually improves by increasing the dimension of the POD space, as confirmed also by the values in Table 1 which gathers the $L^2(\Omega)$ - and of the $H^1(\Omega)$ -norm of the relative modeling error obtained by replacing the HiMod solution $u_{10}(\boldsymbol{\alpha}^*)$ with the HiPOD approximation $u_{\text{HiPOD}}^l(\boldsymbol{\alpha}^*)$, for different values of l . The modeling error quickly reduces by increasing l . From a qualitative viewpoint, the HiPOD approximation $u_{\text{HiPOD}}^{15}(\boldsymbol{\alpha}^*)$ is fully comparable with the HiMod approximation in Figure 1, bottom-right with a reduction of the wall-clock time from 1.44 to 0.04 seconds¹ (the time associated with the HiPOD approximation clearly refers to the online phase only).

	$l = 2$	$l = 4$	$l = 7$	$l = 15$	$l = 17$
$L^2(\Omega)$ -norm	3.23e-01	5.98e-02	3.51e-02	2.70e-03	1.71e-03
$H^1(\Omega)$ -norm	4.50e-01	1.23e-01	6.21e-02	7.61e-03	4.81e-03

Table 1: Basic HiPOD reduction (test case 3): relative modeling error for different HiPOD approximations.

Test case 4

As reference setting, we consider now the test case in Section 2.1.2. We adopt the following dependence on the independent variables for the problem data in (1),

$$\begin{aligned}\mu(\mathbf{x}) &= \mu_0 + \mu_x x + \mu_y y, & \mathbf{b}(\mathbf{x}) &= [b_0, b_1 \sin(6x)]^T, \\ \sigma(\mathbf{x}) &= \sigma_0 + \sigma_x x + \sigma_y y, & f(\mathbf{x}) &= f_1 \chi_{C_1}(\mathbf{x}) + f_2 \chi_{C_2}(\mathbf{x}).\end{aligned}$$

During the offline phase, we compute the HiMod approximation for 30 different ADR problems by setting $\mu_x = \mu_y = \sigma_x = \sigma_y = 0$, and by randomly varying

$$\begin{aligned}\mu_0 &\in \mathcal{P}_{\mu_0} = [0.1, 10], & b_0 &\in \mathcal{P}_{b_0} = [2, 20], & b_1 &\in \mathcal{P}_{b_1} = [1, 3], \\ \sigma_0 &\in \mathcal{P}_{\sigma_0} = [0, 3], & f_1 &\in \mathcal{P}_{f_1} = [5, 25], & f_2 &\in \mathcal{P}_{f_2} = [5, 25],\end{aligned}$$

so that the parameter in (1) is provided by the vector $\boldsymbol{\alpha} = [\mu_0, b_0, b_1, \sigma_0, f_1, f_2]^T$ taking values in the set $\mathcal{P} = \mathcal{P}_{\mu_0} \times \mathcal{P}_{b_0} \times \mathcal{P}_{b_1} \times \mathcal{P}_{\sigma_0} \times \mathcal{P}_{f_1} \times \mathcal{P}_{f_2}$. The HiMod discretization employs linear FE on a uniform partition of Ω_{1D} into 120 subintervals, combined with 20 sinusoidal modes to discretize the transverse dynamics. Figure 3, right shows the trend of the spectrum for the corresponding matrix \mathcal{V} . This exhibits a very slow decay, without any significant drop before the 29-th singular value (being $\text{rank}(\mathcal{V}) = 29$).

¹The computations have been run on a MacBookPro15,3 Intel Core i9 2.40GHz 32 GB desktop computer.

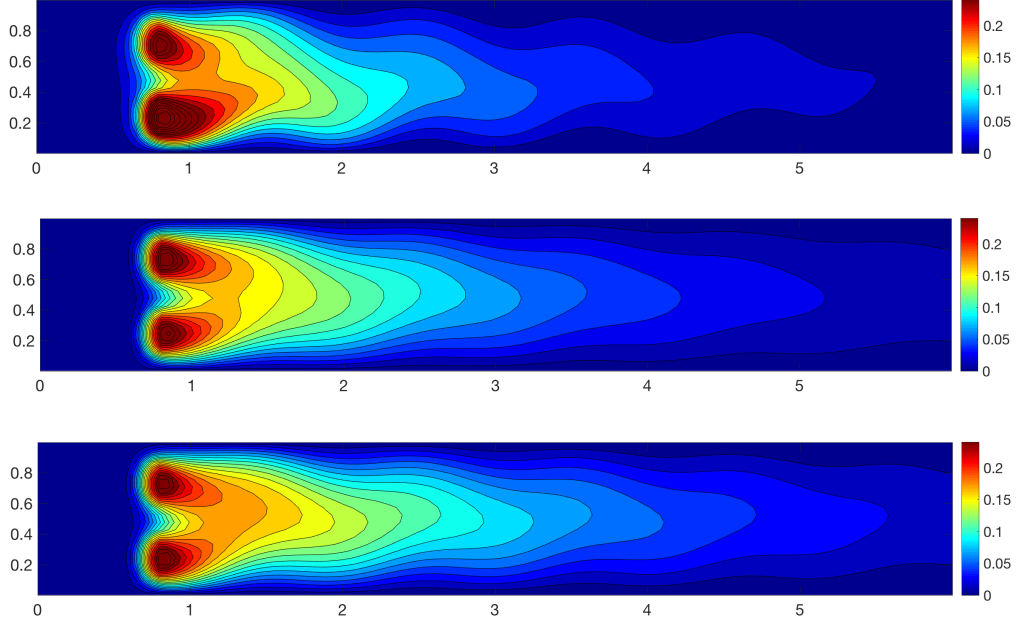


Figure 5: Basic HiPOD reduction (test case 4): HiPOD approximation for $l = 2$ (top), $l = 6$ (center) and $l = 16$ (bottom).

The online phase is employed to approximate the solution to the problem in Section 2.1.2. This is equivalent to set the parameter to

$$\boldsymbol{\alpha}^* = [0.24, 5, 1, 0, 10, 10]^T \in \mathcal{P}.$$

Figure 5, top-bottom shows the HiPOD approximations $u_{\text{HiPOD}}^2(\boldsymbol{\alpha}^*)$, $u_{\text{HiPOD}}^6(\boldsymbol{\alpha}^*)$, $u_{\text{HiPOD}}^{16}(\boldsymbol{\alpha}^*)$. As expected, the ratio R_l becomes closer to 1 when l increases, being $R_2 = 0.6022$, $R_6 = 0.9204$, and $R_{16} = 0.9959$. Six POD modes suffice to recognize already the general trend of the HiMod solution, whereas the HiPOD approximation $u_{\text{HiPOD}}^{16}(\boldsymbol{\alpha}^*)$, which is obtained by solving a system of order 16, is fully comparable with the HiMod approximation $u_5(\boldsymbol{\alpha}^*)$ in Figure 2, bottom, solution to a system of dimension 600. This leads to significant savings in terms of computational effort, the wall-clock time reducing from 14.53 seconds for the HiMod approximation to 0.20 seconds when resorting to the basic HiPOD approach.

Finally, Table 2 provides some quantitative information about the accuracy of the HiPOD approximation, by collecting the $L^2(\Omega)$ - and the $H^1(\Omega)$ -norm of the relative modeling error with respect to the HiMod approximation $u_{20}(\boldsymbol{\alpha}^*)$. The error reduction is slightly slower compared with the values in Table 1, at least until a sufficiently large number of POD modes is employed.

	$l = 2$	$l = 4$	$l = 6$	$l = 8$	$l = 16$	$l = 29$
$L^2(\Omega)$ -norm	2.48e-01	1.98e-01	1.06e-01	3.67e-02	4.11e-03	1.42e-03
$H^1(\Omega)$ -norm	3.39e-01	2.39e-01	1.31e-01	5.52e-02	1.09e-02	3.03e-03

Table 2: Basic HiPOD reduction (test case 4): relative modeling error for different HiPOD approximations.

3.2 The directional HiPOD approach

The directional HiPOD method still combines HiMod reduction with POD, albeit through a more complex procedure. Now, the SVD is employed several times to erase the redundancy along the main stream and the transverse direction, separately, in accordance with the separation of the variables underlying the HiMod approach. Then, the online phase is carried out by means of an interpolation instead of a projection. This relieves us from assembling the HiMod stiffness matrix and right-hand side associated with the online parameter, as expected by (12).

The *offline phase* starts by collecting the information to build the response matrix. To this aim, we compute the HiMod discretization to problem (1) for p different values, α_i , of the parameter α , with $i = 1, \dots, p$. The corresponding modal coefficients, $\{\tilde{u}_{k,j}^{\alpha_i}\}_{k=1,j=1}^{m,N_h}$, are re-ordered by mode into the m vectors

$$\mathbf{U}^k(\alpha_i) = [\tilde{u}_{k,1}^{\alpha_i}, \tilde{u}_{k,2}^{\alpha_i}, \dots, \tilde{u}_{k,N_h}^{\alpha_i}]^T \in \mathbb{R}^{N_h} \quad k = 1, \dots, m, \quad (14)$$

instead of in a unique vector as in (8). Then, we employ vectors $\mathbf{U}^k(\alpha_i)$ to assemble the response matrix

$$U = [\mathbf{U}^1(\alpha_1) \cdots \mathbf{U}^m(\alpha_1) \mid \mathbf{U}^1(\alpha_2) \cdots \mathbf{U}^m(\alpha_2) \mid \cdots \cdots \mid \mathbf{U}^1(\alpha_p) \cdots \mathbf{U}^m(\alpha_p)]$$

$$= \begin{bmatrix} \tilde{u}_{1,1}^{\alpha_1} & \cdots & \tilde{u}_{m,1}^{\alpha_1} & \tilde{u}_{1,1}^{\alpha_2} & \cdots & \tilde{u}_{m,1}^{\alpha_2} & \cdots & \cdots & \tilde{u}_{1,1}^{\alpha_p} & \cdots & \tilde{u}_{m,1}^{\alpha_p} \\ \tilde{u}_{1,2}^{\alpha_1} & \cdots & \tilde{u}_{m,2}^{\alpha_1} & \tilde{u}_{1,2}^{\alpha_2} & \cdots & \tilde{u}_{m,2}^{\alpha_2} & \cdots & \cdots & \tilde{u}_{1,2}^{\alpha_p} & \cdots & \tilde{u}_{m,2}^{\alpha_p} \\ \vdots & \vdots \\ \tilde{u}_{1,N_h}^{\alpha_1} & \cdots & \tilde{u}_{m,N_h}^{\alpha_1} & \tilde{u}_{1,N_h}^{\alpha_2} & \cdots & \tilde{u}_{m,N_h}^{\alpha_2} & \cdots & \cdots & \tilde{u}_{1,N_h}^{\alpha_p} & \cdots & \tilde{u}_{m,N_h}^{\alpha_p} \end{bmatrix}.$$

Matrix $U \in \mathbb{R}^{N_h \times (mp)}$ exhibits a block-wise structure associated with the parameters α_i such that, for each block, columns run over modes while rows run over FE nodes. Now, we apply the SVD to matrix U , thus yielding

$$U = \Xi \Lambda K^T,$$

with $\Xi \in \mathbb{R}^{N_h \times N_h}$ and $K \in \mathbb{R}^{(mp) \times (mp)}$ unitary matrices, and $\Lambda \in \mathbb{R}^{N_h \times (mp)}$ a pseudo-diagonal matrix. The left singular vectors $\{\boldsymbol{\xi}_j\}_{j=1}^{N_h}$ of U constitute an orthogonal basis for \mathbb{R}^{N_h} , so that each column of U can be expanded as

$$\mathbf{U}^k(\alpha_i) = \sum_{j=1}^{N_h} T_j^k(\alpha_i) \boldsymbol{\xi}_j \quad k = 1, \dots, m, \quad i = 1, \dots, p. \quad (15)$$

In general, we can pick the first, say L with $L \leq N_h$, most meaningful singular vectors of U to identify the POD space, $V_{\text{POD},1}^L = \text{span}\{\boldsymbol{\xi}_1, \dots, \boldsymbol{\xi}_L\}$, associated with this first phase of the directional HiPOD procedure, being $\dim(V_{\text{POD},1}^L) = L$. Thus, vectors $\mathbf{U}^k(\alpha_i)$ can be approximated as

$$\mathbf{U}^k(\alpha_i) \cong \sum_{j=1}^L T_j^k(\alpha_i) \boldsymbol{\xi}_j \quad k = 1, \dots, m, \quad i = 1, \dots, p, \quad (16)$$

where equality holds when $L = N_h$ (see (15)). Now, we re-organize coefficients $\{T_j^k(\alpha_i)\}$ by parameter, into the p vectors $\mathbf{T}_j(\alpha_i) = [T_j^1(\alpha_i), \dots, T_j^m(\alpha_i)]^T \in \mathbb{R}^m$ with $i = 1, \dots, p$, and we define the matrix

$$S_j = [\mathbf{T}_j(\alpha_1), \dots, \mathbf{T}_j(\alpha_p)] = \begin{bmatrix} T_j^1(\alpha_1) & \dots & T_j^1(\alpha_p) \\ \vdots & & \vdots \\ T_j^m(\alpha_1) & \dots & T_j^m(\alpha_p) \end{bmatrix} \in \mathbb{R}^{m \times p},$$

with $j = 1, \dots, L$. Then, we apply the SVD to each matrix S_j to obtain the L factorizations

$$S_j = R_j D_j P_j^T, \quad (17)$$

with $R_j \in \mathbb{R}^{m \times m}$ and $P_j \in \mathbb{R}^{p \times p}$ unitary matrices, and $D_j \in \mathbb{R}^{m \times p}$ the pseudo-diagonal matrix collecting the singular values of S_j . Thus, columns $\mathbf{T}_j(\alpha_i)$ of S_j can be represented in terms of the POD orthogonal basis $\{\mathbf{r}_j^k\}_{k=1}^{\mu_j}$, with $\mu_j \leq m$, constituted by the most significant μ_j left singular vectors of S_j , as

$$\mathbf{T}_j(\alpha_i) \cong \sum_{k=1}^{\mu_j} Q_j^k(\alpha_i) \mathbf{r}_j^k \quad j = 1, \dots, L, \quad i = 1, \dots, p. \quad (18)$$

With each j , we associate the POD space $V_{\text{POD},2,j}^{\mu_j} = \text{span}\{\mathbf{r}_j^1, \dots, \mathbf{r}_j^{\mu_j}\}$, with $\dim(V_{\text{POD},2,j}^{\mu_j}) = \mu_j$. Thus, the directional HiPOD procedure yields $(L+1)$ POD bases which, during the online phase, are employed to predict the HiMod approximation to problem (1) for a new value, α^* , of the parameter, with $\alpha^* \neq \alpha_i$ for $i = 1, \dots, p$. For this purpose, first we compute an approximation for the coefficients $Q_j^k(\alpha^*)$ in (18), for $j = 1, \dots, L$ and $k = 1, \dots, \mu_j$, via a suitable interpolation of the (known) values $Q_j^k(\alpha_i)$ for $i = 1, \dots, p$; successively, we go through the directional procedure backward, until obtaining an approximation for the vector $\mathbf{U}^k(\alpha^*)$ in (14). In particular, thanks to (18), we compute the L vectors

$$\mathbf{T}_j(\alpha^*) = [T_j^1(\alpha^*), \dots, T_j^m(\alpha^*)]^T = \sum_{k=1}^{\mu_j} Q_j^k(\alpha^*) \mathbf{r}_j^k \quad j = 1, \dots, L \quad (19)$$

in \mathbb{R}^m , and then, according to (16), we assemble the m vectors $\mathbf{U}_{\text{HiPOD}}^k(\alpha^*) \in \mathbb{R}^{N_h}$ as

$$\mathbf{U}_{\text{HiPOD}}^k(\alpha^*) = [u_{\text{POD},k,1}^{\alpha^*}, \dots, u_{\text{POD},k,N_h}^{\alpha^*}]^T = \sum_{j=1}^L T_j^k(\alpha^*) \boldsymbol{\xi}_j \quad k = 1, \dots, m.$$

Finally, vectors $\mathbf{U}_{\text{HiPOD}}^k(\alpha^*)$ allow us to approximate the HiMod solution $u_m(\alpha^*)$ as

$$u_m(\alpha^*) \approx u_{\text{HiPOD}}^{L, M_L}(\alpha^*) = \sum_{k=1}^m \left[\sum_{j=1}^{N_h} u_{\text{POD}, k, j}^{\alpha^*} \vartheta_j(x) \right] \varphi_k(\psi_x(\mathbf{y})),$$

with $M_L = \{\mu_j\}_{j=1}^L$, and where values $u_{\text{POD}, k, j}^{\alpha^*}$ provide an approximation of the actual coefficient $\tilde{u}_{k, j}^{\alpha^*}$ in (14) with $\alpha_i = \alpha^*$.

Remark 3.3 (Role of the two levels) *The singular value decomposition of the matrix U , at the first level, mixes information about the HiMod coefficients at different finite element nodes; on the other hand, the singular value decomposition of matrices S_j 's, at the second level, reveals a possible redundancy of information for the coefficients needed to describe the changes of the HiMod solution over different parameter configurations. Therefore, one would expect that mild changes of the HiMod coefficients across different values of the parameter lead to rank deficient matrices S_j 's, which would translate in potentially little loss of accuracy when a dimensionality reduction is performed accordingly.*

To validate this conjecture, we set up a numerical test. At the i -th run of the offline phase, we solve a Poisson problem completed with homogeneous Dirichlet boundary conditions on the domain $\Omega = (0, L_x) \times (0, L_y)$, so that the exact solution is $u_i(x, y) = x(x - L_x) \left[\sum_{m=1}^i \sin\left(\frac{m\pi y}{L_y}\right) \right]$. The parameter governing the offline phase is the number i of HiMod modes used to reconstruct the solution u_i in exact arithmetic and, clearly, the complexity of the solution increases with i . Because solutions of different problems require a different number of HiMod modes, the accuracy of the HiPOD approximation is expected to be highly sensitive to the dimensionality reduction performed. Now, we employ the online phase to recover the solution u_i , for a random value of i , via the directional HiPOD reduction, and to measure the associated (relative) error (see Table 3). This analysis shows that the accuracy obtained with the HiPOD approximation is not sensitive to the threshold on the first level, but it is with respect to the threshold at the second level. This is reasonable, as the second level retains information about the importance of the HiMod modes in reconstructing the solution and how these modes vary through the parameter space spanned in the offline phase. Moreover, it can be noticed that matrices S_j 's exhibit an upper triangular pattern, due to the growing complexity of the solution.

Remark 3.4 (Choice of the interpolation) *Different interpolation procedures can be adopted to compute coefficients $Q_j^k(\alpha^*)$. Following [37], we adopt a standard linear interpolation, a piecewise cubic Hermite interpolant and an interpolating radial basis function. In the next section, we numerically investigate the performances of these three approaches.*

		$\varepsilon_2 = 0.6$	$\varepsilon_2 = 0.9$	$\varepsilon_2 = 0.99$
$\varepsilon_1 = 0.6$	$L^2(\Omega)$ -norm	8.97e+00	2.54e+00	3.29e-04
	$H^1(\Omega)$ -norm	9.16e+01	4.41e+01	4.99e-02
$\varepsilon_1 = 0.9$	$L^2(\Omega)$ -norm	8.97e+00	2.54e+00	3.29e-04
	$H^1(\Omega)$ -norm	9.16e+01	4.41e+01	4.99e-02
$\varepsilon_1 = 0.99$	$L^2(\Omega)$ -norm	8.97e+00	2.54e+00	3.29e-04
	$H^1(\Omega)$ -norm	9.16e+01	4.41e+01	4.99e-02

Table 3: Directional HiPOD reduction: relative modeling error for different choices of the tolerances to investigate the role of the two levels.

3.2.1 Numerical assessment

We numerically assess the reliability of the directional HiPOD procedure. First, we consider the case where α coincides with a single scalar quantity; then, we generalize the approach to the vector case, so that α will collect more parameters.

Test case 5

We adopt the solution to Test case 1 as the setting to be approximated during the online phase. The viscosity coefficient, μ , which is here assumed constant, represents the parameter driving the offline phase, so that $\alpha = \mu$. In particular, we hierarchically reduce problem (1)-(2) for 20 different values of μ , with $\mu = \mu_i$ uniformly sampled in the interval $\mathcal{P}_\mu = [0.15, 3]$ and $\mu_i \neq 1$ for $i = 1, \dots, 20$, while preserving the same values as in (6) for the other problem data. The HiMod discretization is the same as adopted for Test case 3, so that we employ linear FE, associated with a uniform partition of Ω_{1D} into 60 subintervals, to discretize the main stream and 10 sinusoidal modes to describe the transverse dynamics.

Concerning the choice of L in (16) and of μ_i in (18), we resort to a control analogous to the one in (11). In more detail, for two fixed tolerances, ε_1 and ε_2 , with $0 \leq \varepsilon_1, \varepsilon_2 \leq 1$, we preserve the first L left singular vectors, ξ_j , of U and the first μ_j left singular vectors, \mathbf{r}_j^k , of S_j such that

$$R_{\text{POD},1}^L = \frac{\sum_{j=1}^L \lambda_j^2}{\sum_{j=1}^{N_h} \lambda_j^2} \geq \varepsilon_1 \quad \text{and} \quad R_{\text{POD},2}^{\mu_j} = \frac{\sum_{k=1}^{\mu_j} d_{j,k}^2}{\sum_{k=1}^m d_{j,k}^2} \geq \varepsilon_2, \quad (20)$$

respectively, with λ_j the singular value of U associated with ξ_j and $j = 1, \dots, N_h$, and with $d_{j,k}$ the singular value of S_j corresponding to the k -th singular vector \mathbf{r}_j^k and $k = 1, \dots, m$. As a first check, we choose $\varepsilon_1 = \varepsilon_2 = \varepsilon$. In particular, Table 4 collects the predictions for L , for the maximum value and for the median of the values μ_j , for different choices of ε . As expected, the number of Hi-POD modes retained at both stages increases when ε approaches 1. Moreover, a higher sensitivity of L to the

	$\varepsilon = 0.6$	$\varepsilon = 0.9$	$\varepsilon = 0.99$	$\varepsilon = 0.999$	$\varepsilon = 0.9999$
L	1	3	5	7	10
$\max_j \mu_j$	4	6	8	9	10
median μ_j	2	4	6	8	8

Table 4: Directional HiPOD reduction (test case 5): prediction for the POD modes.

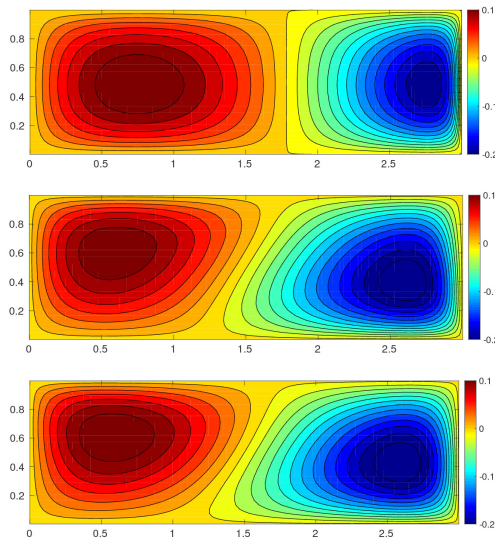


Figure 6: Directional HiPOD reduction (test case 5): HiPOD approximation for $\varepsilon = 0.6$ (top), $\varepsilon = 0.9$ (middle) and $\varepsilon = 0.99$ (bottom).

selected tolerance is detected, when compared with the maximum value and the median of μ_j 's.

The online phase is performed by setting $\alpha^* = \mu^* = 1 \in \mathcal{P}_\mu$, and by using a radial basis function (RBF) interpolation [38]. In Figure 6, we compare the HiPOD approximations associated with three of the selected tolerances. It is noticed that, at the first level of the procedure, at least three POD modes have to be adopted to have an approximation sufficiently reliable, which is equivalent to pick $\varepsilon \geq 0.9$. On average, the wall-clock time required by the directional HiPOD procedure is 0.08 seconds. This time is fully comparable with the one associated with the basic HiPOD approach (0.04 seconds) and it is still considerably lower when compared with the wall-clock time demanded by a HiMod reduction.

In Table 5, we analyze the convergence of the directional HiPOD approach, by computing the $L^2(\Omega)$ - and the $H^1(\Omega)$ -norm of the relative error obtained by replacing the HiMod solution $u_{10}(\alpha^*)$ with the HiPOD approximation. Although a cross-comparison between the basic and the directional HiPOD reduction techniques is not straightforward due to the heterogeneity of the two approaches, we observe that the

accuracy reached in Table 5 is higher with respect to the one ensured by Table 2. Additionally, in order to estimate the maximum accuracy provided by the two methods, we compute the error for both the HiPOD approximations when all the POD modes are used (i.e., $l = mN_h$ for the basic approach, $L = N_h$ and $\mu_j = m$ in (16) and (18), respectively for the directional case). As Table 6 shows, the directional HiPOD procedure allows us to gain (at least) one order of accuracy with respect to both the $L^2(\Omega)$ - and the $H^1(\Omega)$ -norm.

	$\varepsilon = 0.6$	$\varepsilon = 0.9$	$\varepsilon = 0.99$	$\varepsilon = 0.999$	$\varepsilon = 0.9999$
$L^2(\Omega)$ -norm	4.66e-01	4.01e-02	3.11e-03	8.17e-04	1.37e-04
$H^1(\Omega)$ -norm	4.62e-01	9.43e-02	1.05e-02	3.11e-03	5.71e-04

Table 5: Directional HiPOD reduction (test case 5): relative modeling error for different HiPOD approximations.

	basic HiPOD	directional HiPOD	basic HiPOD	directional HiPOD
$L^2(\Omega)$ -norm	1.71e-03	1.35e-04	1.42e-03	7.48e-05
$H^1(\Omega)$ -norm	4.81e-03	2.20e-04	3.03e-03	4.20e-04

Table 6: Cross comparison between basic and directional HiPOD procedures: relative modeling error for test case 4 (first and second column) and for test case 5 (third and fourth column).

Finally, we run the directional HiPOD procedure by distinguishing the tolerances in (20), in order to identify a possible criterion of choice for ε_1 and ε_2 . To this goal, we repeat the same error analysis as in Table 5, varying both ε_1 and ε_2 in the set of values $\{0.6, 0.9, 0.99, 0.999, 0.9999\}$. Table 7 collects the results of this investigation. It turns out that the values of ε_1 and ε_2 have to be, in general, sufficiently close to 1 to have a monotonically decreasing trend of the error when we fix a tolerance and vary the other one. For this particular test case, a possible strategy to ensure this monotonicity can be to select ε_1 very close to 1 ($\varepsilon_1 = 0.9999$) and make ε_2 varying, or, as an alternative, we can fix ε_2 to 0.99, 0.999 or 0.9999 and gradually reduce the value for ε_1 . This behaviour is shared by both the norms.

Test case 6

The benchmark configuration is now provided by Test case 2, where the HiPOD parameter α , coincides with the viscosity coefficient μ that we assume constant in this case.

The offline phase involves the hierarchically reduction of problem (1)-(2) for ten different values of the viscosity, uniformly sampled in the range $\mathcal{P}_\mu = [1/30, 1]$, and all the other problem data in (7) are preserved. The HiMod discretization adopted during this stage uses linear FE along Ω_{1D} , in correspondence with a uniform partition of

		$\varepsilon_2 = 0.6$	$\varepsilon_2 = 0.9$	$\varepsilon_2 = 0.99$	$\varepsilon_2 = 0.999$	$\varepsilon_2 = 0.9999$
$\varepsilon_1 = 0.6$	$L^2(\Omega)$ -norm	2.58e-01	2.58e-01	2.57e-01	2.57e-01	2.57e-01
	$H^1(\Omega)$ -norm	4.61e-01	4.61e-01	4.59e-01	4.59e-01	4.59e-01
$\varepsilon_1 = 0.9$	$L^2(\Omega)$ -norm	5.43e-02	5.43e-02	2.01e-02	2.01e-02	2.01e-02
	$H^1(\Omega)$ -norm	1.50e-01	1.50e-01	5.91e-02	5.88e-02	5.88e-02
$\varepsilon_1 = 0.99$	$L^2(\Omega)$ -norm	3.73e-02	3.47e-02	5.80e-03	5.80e-03	5.80e-03
	$H^1(\Omega)$ -norm	8.90e-02	7.57e-02	2.83e-02	2.83e-02	2.83e-02
$\varepsilon_1 = 0.999$	$L^2(\Omega)$ -norm	3.72e-02	3.46e-02	1.34e-03	6.03e-04	6.03e-04
	$H^1(\Omega)$ -norm	8.85e-02	7.51e-02	4.01e-03	3.10e-03	2.91e-03
$\varepsilon_1 = 0.9999$	$L^2(\Omega)$ -norm	3.72e-02	3.46e-02	1.20e-03	5.57e-04	8.03e-05
	$H^1(\Omega)$ -norm	8.84e-02	7.50e-02	2.81e-03	1.21e-03	3.95e-04

Table 7: Directional HiPOD reduction (test case 5): sensitivity to the selected tolerances.

the supporting fiber into 120 subintervals, and 20 sinusoidal modes in the transverse direction, analogously to what done in Test case 4.

We set $\alpha^* = 0.24 \in \mathcal{P}_\mu$ in the online phase to recover the setting of interest. The spectrum truncation in (20) is first driven by a unique tolerance, by selecting $\varepsilon_1 = \varepsilon_2 = \varepsilon$.

The first row in Table 8 provides the number, L , of POD modes selected at the first level of the HiPOD procedure, for five different choices of ε . The values in the table highlight the presence of a strong redundancy. Indeed, L is considerably lower with respect to N_h ($= 120$), even when ε is very close to 1. For instance, it suffices that the POD space $V_{\text{POD},1}^L$ has a dimension equal to 13, to correctly describe the dynamics along the main stream, as shown in Figure 7 which gathers the contour plots of the HiPOD approximation for the three smallest values of ε . In general, the configuration explored in this test case is more complex when compared with the one in Test case 5, where three POD modes at the first level are enough to ensure a reliable HiPOD solution.

Also the values predicted for the dimensions μ_j in (18) are contained (see the second row in Table 8). The wall-clock time required by the directional HiPOD procedure (on average, 0.31 seconds) is comparable with the one taken by the basic HiPOD technique (0.20 seconds), and still significantly smaller with respect to the time associated with the HiMod approximation.

	$\varepsilon = 0.6$	$\varepsilon = 0.9$	$\varepsilon = 0.99$	$\varepsilon = 0.999$	$\varepsilon = 0.9999$
L	2	4	13	24	35
$\max_j \mu_j$	5	9	12	14	18
median μ_j	4	7	9	11	12

Table 8: Directional HiPOD reduction (test case 6): prediction for the POD modes.

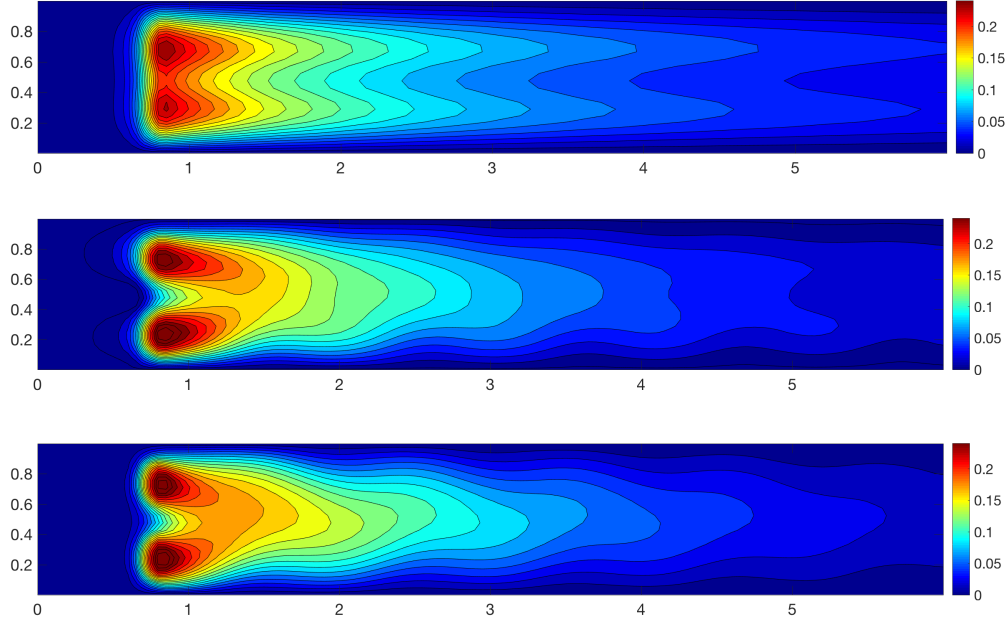


Figure 7: Directional HiPOD reduction (test case 6): HiPOD approximation for $\varepsilon = 0.6$ (top), $\varepsilon = 0.9$ (center) and $\varepsilon = 0.99$ (bottom).

	$\varepsilon = 0.6$	$\varepsilon = 0.9$	$\varepsilon = 0.99$	$\varepsilon = 0.999$	$\varepsilon = 0.9999$
$L^2(\Omega)$ -norm	2.06e-01	7.74e-02	4.41e-03	3.27e-04	7.48e-05
$H^1(\Omega)$ -norm	4.72e-01	2.04e-01	2.31e-02	1.82e-03	4.20e-04

Table 9: Directional HiPOD reduction (test case 6): relative modeling error for different HiPOD approximations.

The accuracy of the directional HiPOD approximation is quantified in Table 9, in terms of the $L^2(\Omega)$ - and of the $H^1(\Omega)$ -norm of the POD relative error with respect to the HiMod solution $u_{20}(\alpha^*)$. The HiPOD procedure turns out to be very effective by ensuring to reach a smaller error when compared with the values in Table 2. This is corroborated by the third and fourth columns in Table 6, where the comparison between the basic and the directional HiPOD procedures is carried out when exploiting the whole POD bases.

Also for this test configuration, we explore the accuracy of the directional HiPOD approximation when we differently select ε_1 and ε_2 . The analysis in Table 9 is replicated, by assigning the values 0.6, 0.9, 0.99, 0.999, 0.9999 to both the tolerances. Table 10 provides the relative modeling error with respect to the reference HiMod solution in terms of the $L^2(\Omega)$ - and of the $H^1(\Omega)$ -norms. Conclusions similar to the ones for Table 7 can be drawn also for this test case. To ensure a monotonic trend for the error norm, it is fundamental to choose ε_1 very close to 1 ($\varepsilon_1 = 0.999$ or $\varepsilon_1 = 0.9999$)

and gradually reduce ε_2 , or, as an alternative, to set ε_2 to 0.99, 0.999 or 0.999, while diminishing ε_1 .

		$\varepsilon_2 = 0.6$	$\varepsilon_2 = 0.9$	$\varepsilon_2 = 0.99$	$\varepsilon_2 = 0.999$	$\varepsilon_2 = 0.9999$
$\varepsilon_1 = 0.6$	$L^2(\Omega)$ -norm	2.06e-01	1.52e-01	1.42e-01	1.42e-01	1.42e-01
	$H^1(\Omega)$ -norm	4.72e-01	3.26e-01	3.09e-01	3.09e-01	3.09e-01
$\varepsilon_1 = 0.9$	$L^2(\Omega)$ -norm	1.61e-01	7.74e-02	5.56e-02	5.55e-02	5.55e-02
	$H^1(\Omega)$ -norm	3.90e-01	2.04e-01	1.68e-01	1.67e-01	1.67e-01
$\varepsilon_1 = 0.99$	$L^2(\Omega)$ -norm	1.52e-01	5.40e-02	4.40e-03	3.31e-03	3.31e-03
	$H^1(\Omega)$ -norm	3.52e-01	1.29e-01	2.31e-02	2.21e-02	2.21e-02
$\varepsilon_1 = 0.999$	$L^2(\Omega)$ -norm	1.52e-01	5.39e-02	2.91e-03	1.81e-03	1.72e-03
	$H^1(\Omega)$ -norm	3.51e-01	1.27e-01	7.31e-03	3.27e-04	2.71e-04
$\varepsilon_1 = 0.9999$	$L^2(\Omega)$ -norm	1.52e-01	5.34e-02	2.90e-03	1.98e-04	7.48e-05
	$H^1(\Omega)$ -norm	3.51e-01	1.27e-01	7.11e-03	8.99e-04	4.21e-04

Table 10: Directional HiPOD reduction (test case 6): sensitivity to the selected tolerances.

Finally, we use this test case to investigate the sensitivity of the directional HiPOD reduction procedure to the interpolant used to compute the coefficients $Q_j^k(\alpha^*)$ in (19). For this purpose, we consider the four largest tolerances since $\varepsilon = 0.6$ provides an excessively poor approximation. According to Remark 3.4, we resort to a standard linear interpolation (LIN), a piecewise cubic Hermite (PCH) interpolant and to an interpolating RBF. Table 11 provides the $L^2(\Omega)$ - and the $H^1(\Omega)$ -norm of the relative error associated with the directional HiPOD approximation with respect to the HiMod solution $u_{20}(\alpha^*)$. The PCH and the RBF interpolants outperform the linear interpolation, especially when a higher accuracy is required, with a slightly better performance for the RBF approach.

		$\varepsilon = 0.9$	$\varepsilon = 0.99$	$\varepsilon = 0.999$	$\varepsilon = 0.9999$
LIN	$L^2(\Omega)$ -norm	7.74e-02	4.43e-03	1.56e-03	1.51e-03
	$H^1(\Omega)$ -norm	2.04e-01	2.32e-02	2.51e-03	1.77e-03
PCH	$L^2(\Omega)$ -norm	7.74e-02	4.41e-03	3.56e-04	1.60e-04
	$H^1(\Omega)$ -norm	2.04e-01	2.31e-03	1.92e-03	5.33e-04
RBF	$L^2(\Omega)$ -norm	7.74e-02	4.44e-03	3.27e-04	7.48e-05
	$H^1(\Omega)$ -norm	2.04e-01	2.31e-02	1.81e-03	4.20e-04

Table 11: Directional HiPOD reduction (test case 6): sensitivity to the interpolant operator.

Test case 7

We analyze here the robustness of the directional HiPOD procedure in terms of extrapolation, to predict a scenario associated with a value, α^* , of the parameter out of the

range \mathcal{P} . The configuration selected for this check is the same as for Test case 6, where, now, we pick $\alpha^* = 1/60 \notin \mathcal{P}_\mu$. We exploit the offline phase of the previous test case, and then, for comparison purposes, we adopt both the PCH and the RBF interpolations to compute coefficients $Q_j^k(\alpha^*)$ in (19). This choice is motivated by the higher reliability exhibited, in general, by these two interpolants in terms of extrapolation properties. Table 12 compares the modeling relative error associated with the two interpolants, in terms of the $L^2(\Omega)$ - and the $H^1(\Omega)$ -norms. PCH and RBF procedures are fully comparable, with a slightly better performance for the second interpolant. Figure 8 shows the contour plots of the reference HiMod solution, $u_{20}(\alpha^*)$, and of the directional HiPOD approximation when resorting to the RBF interpolant and for $\varepsilon_1 = \varepsilon_2 = \varepsilon = 0.9$ and 0.99 (tolerances $\varepsilon = 0.999, 0.9999$ provide contour plots very similar to the bottom panel). The difficulty intrinsic in an extrapolation procedure is confirmed by the value to be picked for ε which has to be very close to 1 in order to yield a reliable HiPOD solution.

		$\varepsilon = 0.9$	$\varepsilon = 0.99$	$\varepsilon = 0.999$	$\varepsilon = 0.9999$
PCH	$L^2(\Omega)$ -norm	2.75e-01	1.01e-01	9.79e-02	9.78e-02
	$H^1(\Omega)$ -norm	5.46e-01	2.13e-01	1.92e-01	1.92e-01
RBF	$L^2(\Omega)$ -norm	2.67e-01	5.31e-02	4.70e-02	4.68e-02
	$H^1(\Omega)$ -norm	5.36e-01	1.44e-01	1.02e-01	9.97e-02

Table 12: Directional HiPOD reduction (test case 7): robustness to extrapolation.

Test case 8

In this section we extend the HiPOD directional approach to the case of multiple parameters to be varied during the offline phase. The use of a vector of parameters leads us to modify only the interpolation step of the procedure in Section 3.2, which now involves a two-dimensional interpolant in order to recover coefficients $Q_j^k(\alpha^*)$ in (19).

As a reference differential setting, we adopt the ADR problem in Test case 2, where we identify the parameter with the vector $\alpha = [\mu, b_1]^T$ which collects the diffusivity coefficient and the x -component of the advective field, $\mathbf{b} = [b_1, b_2]^T$, the y -component being preserved as in (7) (i.e., $b_2 = \sin(6x)$). The set of the admissible parameters is $\mathcal{P} = \mathcal{P}_\mu \times \mathcal{P}_{b_1}$, with $\mathcal{P}_\mu = [1/30, 1]$ and $\mathcal{P}_{b_1} = [0.5, 10]$.

Due to the higher dimensionality of the parameter space, we extend the sampling during the offline phase, by hierarchically reducing the ADR problem for $p = 600$ different choices of the parameter α . In particular, the interval \mathcal{P}_μ is sampled with 30 uniformly distributed points, whereas we pick 20 uniformly spaced points along the interval \mathcal{P}_{b_1} . The HiMod approximation coincides with the one adopted for Test cases 4 and 6, which employs a linear finite element discretization associated with a uniform subdivision of Ω_{1D} into 120 subintervals along the mainstream, enriched by 20 sinusoidal modal functions to approximate the transverse dynamics.

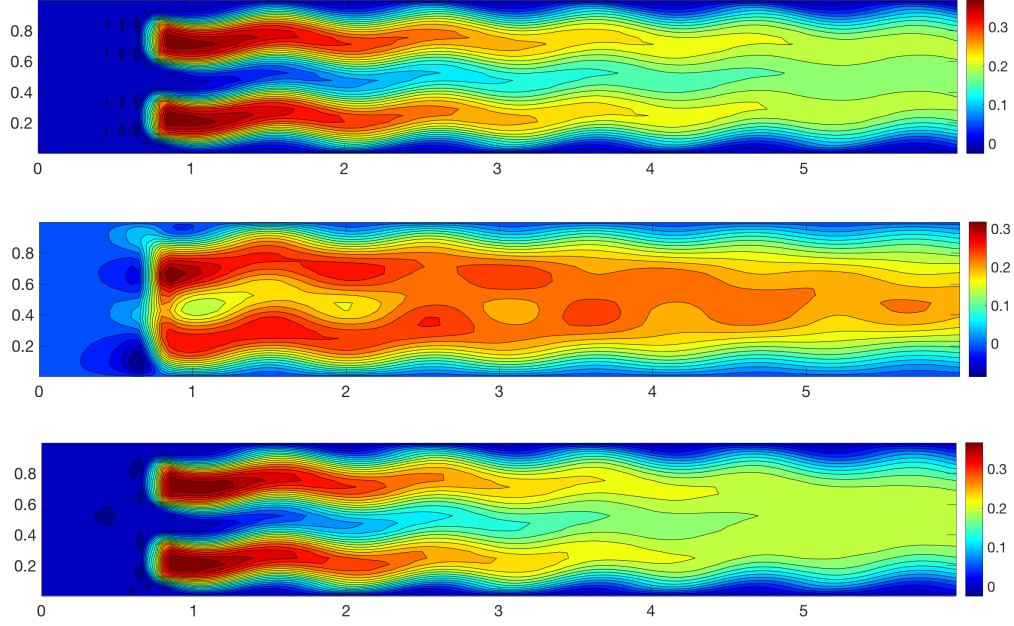


Figure 8: Directional HiPOD reduction (test case 7): robustness to extrapolation. HiMod reference solution (top) and HiPOD approximation for $\varepsilon = 0.9$ (center) and $\varepsilon = 0.99$ (bottom).

The POD truncation is carried out by identifying the two tolerances in (20), and by setting $\varepsilon = \varepsilon_1 = \varepsilon_2 = 0.6, 0.9, 0.99, 0.999, 0.9999$.

The online phase is run to approximate the HiMod solution corresponding to the choices $\alpha_1^* = [0.6, 5.1]^T$ and $\alpha_2^* = [0.06, 9.3]^T$ for the parameter. Concerning the interpolation step, we adopt both the linear (LIN) and the piecewise cubic Hermite (PCH) bidimensional interpolant operators. In Figures 9 and 10 we compare the reference HiMod solutions, $u_{20}(\alpha_1^*)$ and $u_{20}(\alpha_2^*)$, with the approximation provided by the directional HiPOD reduction when combined with the PCH interpolation, and for the different tolerances. A tolerance sufficiently close to 1 has to be selected to obtain a reliable HiPOD solution. In particular, the choice α_2^* for the parameter turns out to be particularly challenging for the HiPOD procedure (this is confirmed also by a cross-comparison between the values in Tables 13 and 14).

Tables 13 and 14 offer more quantitative information, by gathering the $L^2(\Omega)$ - and the $H^1(\Omega)$ -norm of the relative modeling error associated with the directional HiPOD approximation. For the first choice of the parameter, $\alpha_1^* = [0.6, 5.1]^T$, it is not easy to appreciate a remarkable difference between the two interpolants until the tolerance becomes very close to 1. On the contrary, the parameter $\alpha_2^* = [0.06, 9.3]^T$ highlights the better performances of the PCH interpolation in terms of both the norms.

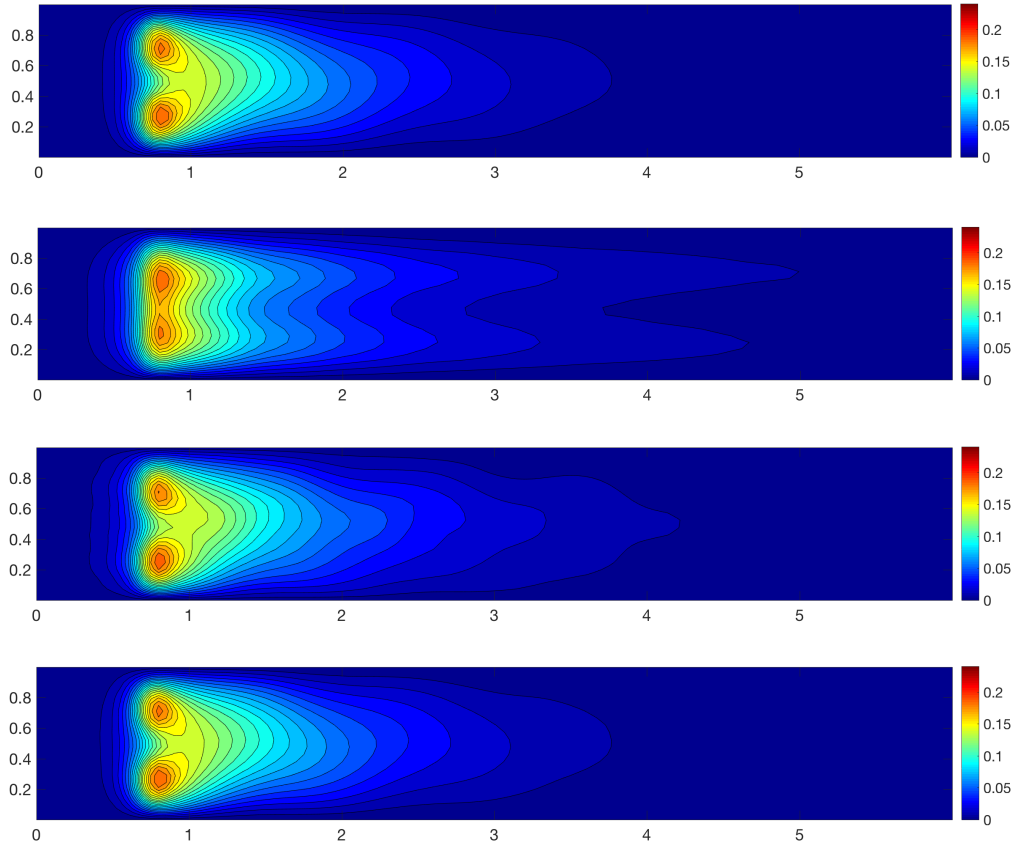


Figure 9: Directional HiPOD reduction (test case 8) for $\alpha_1^* = [0.6, 5.1]^T$: HiMod solution (first row) and HiPOD approximation associated with the PCH interpolant, and for $\varepsilon = 0.6$ (second row), $\varepsilon = 0.9$ (third row), $\varepsilon = 0.99$ (fourth row).

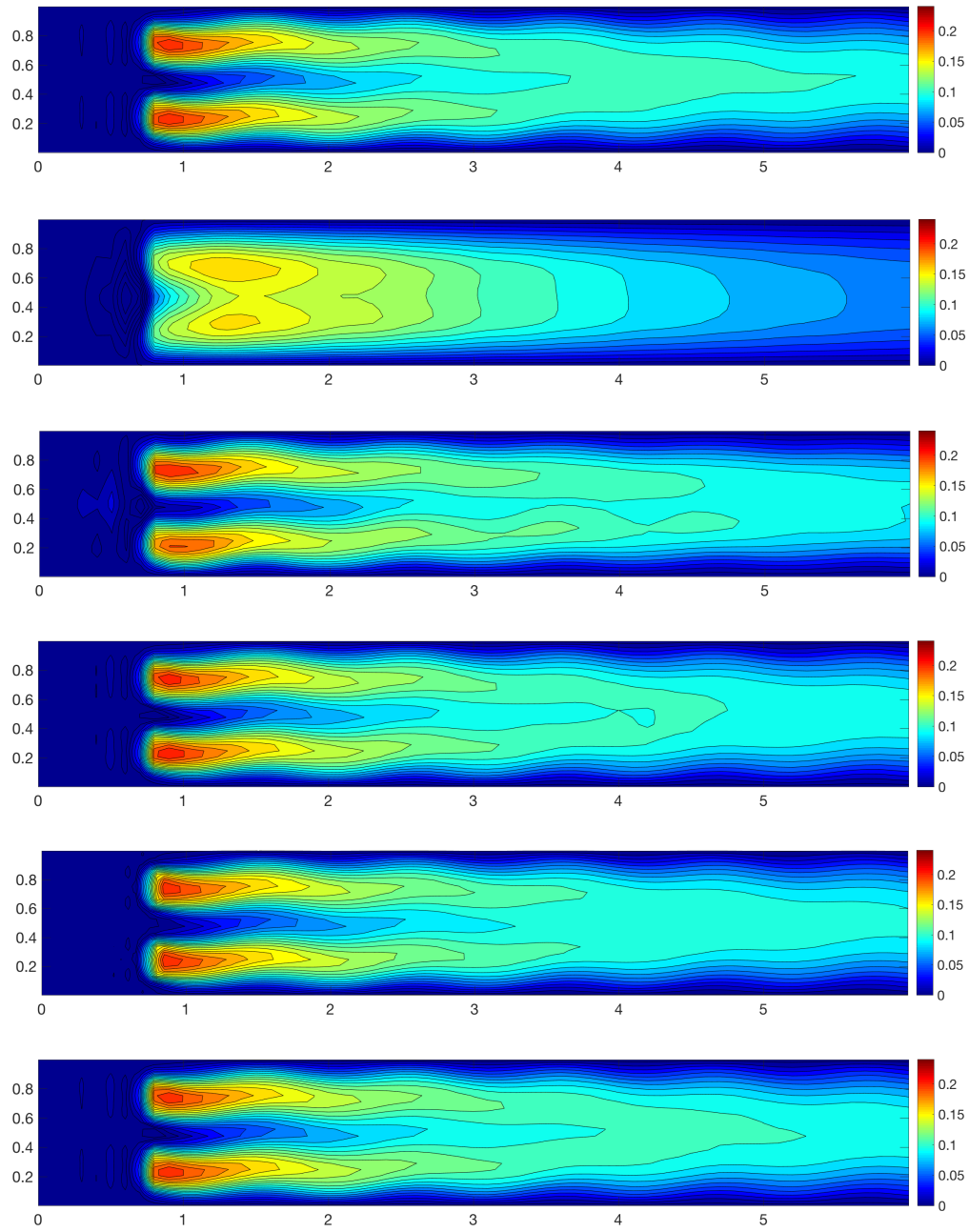


Figure 10: Directional HiPOD reduction (test case 8) for $\alpha_2^* = [0.06, 9.3]^T$: HiMod solution (first row) and HiPOD approximation associated with the PCH interpolant, and for $\varepsilon = 0.6$ (second row), $\varepsilon = 0.9$ (third row), $\varepsilon = 0.99$ (fourth row), $\varepsilon = 0.999$ (fifth row) and $\varepsilon = 0.9999$ (sixth row).

		$\varepsilon = 0.6$	$\varepsilon = 0.9$	$\varepsilon = 0.99$	$\varepsilon = 0.999$	$\varepsilon = 0.9999$
	L	2	6	16	32	41
	$\max_j \mu_j$	7	13	19	20	20
	median μ_j	5	10	16	19	20
LIN	$L^2(\Omega)$ -norm	1.81e-01	5.13e-02	3.81e-03	6.33e-04	5.71e-04
	$H^1(\Omega)$ -norm	3.90e-01	1.37e-01	1.74e-02	2.10e-03	6.34e-04
PCH	$L^2(\Omega)$ -norm	1.82e-01	5.13e-02	3.72e-03	2.78e-04	4.23e-05
	$H^1(\Omega)$ -norm	3.90e-01	1.37e-01	1.74e-02	2.01e-03	2.51e-04

Table 13: Directional HiPOD reduction (test case 8): relative modeling error for different HiPOD approximations and sensitivity to the interpolant operator for $\alpha_1^* = [0.6, 5.1]^T$.

		$\varepsilon = 0.6$	$\varepsilon = 0.9$	$\varepsilon = 0.99$	$\varepsilon = 0.999$	$\varepsilon = 0.9999$
	L	2	6	16	32	41
	$\max_j \mu_j$	7	13	19	20	20
	median μ_j	5	10	16	19	20
LIN	$L^2(\Omega)$ -norm	2.92e-01	5.89e-02	1.49e-02	1.25e-02	1.25e-02
	$H^1(\Omega)$ -norm	5.34e-01	1.73e-01	4.48e-02	2.76e-02	2.76e-02
PCH	$L^2(\Omega)$ -norm	2.93e-01	5.76e-02	9.22e-03	4.30e-03	4.14e-03
	$H^1(\Omega)$ -norm	5.24e-01	1.70e-01	3.62e-02	1.21e-02	9.53e-03

Table 14: Directional HiPOD reduction (test case 8): relative modeling error for different HiPOD approximations and sensitivity to the interpolant operator for $\alpha_2^* = [0.06, 9.3]^T$.

4 Conclusions and developments

The numerical assessment in Sections 3.1.1 and 3.2.1 corroborates the reliability of the two HiPOD reduction procedures. In particular, a more extensive check has been performed on the directional approach, being the less straightforward one and representing the main novelty of the paper. We have analyzed the performances of the directional HiPOD procedure in terms of convergence, selection of the tolerances driving the truncation of the POD bases, choice of the interpolant operator, and robustness with respect to the extrapolation and a multi-parameter context.

The cross-comparison between the two HiPOD methods confirms the greater potential of the directional variant, which, in Table 6, allows us to gain at least one order of accuracy with respect to the basic technique, with respect to both the $L^2(\Omega)$ - and the $H^1(\Omega)$ -norms. Despite both the HiPOD procedures deserving a more thorough investigation in 3D and on more generic geometries, we believe that HiPOD model reduction represents a promising tool. For instance, HiPOD could be used to effectively manage

multi-query contexts such as inverse problems, optimization strategies, data assimilation techniques, parameter estimation algorithms. Therefore, HiPOD could become a potential competitor against renowned techniques, such as the reduced basis method and the Proper Generalized Decomposition (PGD) (we refer to [27], where a first attempt of comparing HiMod/HiPOD reduction with PGD is carried out).

Moreover, we notice that the technique we propose is fully general. In fact, we can employ as the “truth” any reliable reduced model, as well as we can adopt methods other than POD to generate the reduced basis. In [39], for instance, the authors apply a reduced basis approach to collect the high-fidelity information and use a greedy algorithm to extract the essential information.

As for the possible future research topics, we mention the proposal of rigorous estimators to drive the POD selection ([18, 35]), the generalization to a nonlinear framework where an empirical (discrete) interpolation ([5, 17, 33]) unavoidably leads to a prohibitive computational burden. In addition, we aim at applying HiPOD reduction techniques to hemodynamic problems to make scientific modeling a crucial decision tool in clinical practice [8, 23].

Acknowledgements

This work used resources of the Oak Ridge Leadership Computing Facility (OLCF), which is a DOE Office of Science User Facility supported under Contract DE-AC05-00OR22725.

The second author acknowledges the European Union’s Horizon 2020 research and innovation programme under the Marie Skłodowska-Curie Actions, grant agreement 872442 (ARIA, Accurate Roms for Industrial Applications), and the research project GNCS-INdAM 2020 “Tecniche Numeriche Avanzate per Applicazioni Industriali”.

References

- [1] M.C. Aletti, S. Perotto, and A. Veneziani. HiMod reduction of advection-diffusion-reaction problems with general boundary conditions. *J. Sci. Comput.*, 76(1):89–119, 2018.
- [2] D. Amsallem and C. Farhat. An online method for interpolating linear parametric reduced-order models. *SIAM J. Sci. Comput.*, 33(5):2169–2198, 2011.
- [3] C. Audouze, F. De Vuyst, and P.B. Nair. Reduced-order modeling of parameterized PDEs using time-space-parameter principal. *Internat. J. Numer. Methods Engrg.*, 80(8):1025–1057, 2009.
- [4] D. Baroli, C.M. Cova, S. Perotto, L. Sala, and A. Veneziani. Hi-POD solution of parametrized fluid dynamics problems: preliminary results. In *Model Reduction of Parametrized Systems*, volume 17 of *MS&A. Model. Simul. Appl.*, pages 235–254. Springer, Cham, 2017.

- [5] M. Barrault, Y. Maday, N.C. Nguyen, and A.T. Patera. An empirical interpolation method: application to efficient reduced-basis discretization of partial differential equations. *C. R. Math. Acad. Sci. Paris*, 339(9):667–672, 2004.
- [6] U. Baur, C.A. Beattie, P. Benner, and S. Gugercin. Interpolatory projection methods for parameterized model reduction. *SIAM J. Sci. Comput.*, 33(5):2489–2518, 2011.
- [7] P. Benner, S. Gugercin, and K. Willcox. A survey of projection-based model reduction methods for parametric dynamical systems. *SIAM Rev.*, 57(4):483–531, 2015.
- [8] Y.A. Brandes Costa Barbosa and S. Perotto. Hierarchically reduced models for the Stokes problem in patient-specific artery segments. *Int. J. Comput. Fluid Dyn.*, 34(2):160–171, 2020.
- [9] C. Canuto, Y. Maday, and A. Quarteroni. Analysis of the combined finite element and Fourier interpolation. *Numer. Math.*, 39(2):205–220, 1982.
- [10] F. Chinesta, R. Keunings, and A. Leygue. *The Proper Generalized Decomposition for Advanced Numerical Simulations: a Primer*. SpringerBriefs in Applied Sciences and Technology. Springer International Publishing, 2014.
- [11] A. Ern and J.-L. Guermond. *Theory and Practice of Finite Elements*, volume 159 of *Applied Mathematical Sciences*. Springer-Verlag, New York, 2004.
- [12] A. Ern, S. Perotto, and A. Veneziani. Hierarchical model reduction for advection-diffusion-reaction problems. In K. Kunisch, G. Of, and O. Steinbach, editors, *Numerical Mathematics and Advanced Applications*, pages 703–710. Springer-Verlag, Berlin Heidelberg, 2008.
- [13] G.H. Golub and C.F. Van Loan. *Matrix Computations*. Johns Hopkins Studies in the Mathematical Sciences. Johns Hopkins University Press, Baltimore, MD, fourth edition, 2013.
- [14] D. González and A. Ammar. Recent advances on the use of separated representations. *Internat. J. Numer. Methods Engrg.*, 81(5):637–659, 2010.
- [15] S. Guzzetti, S. Perotto, and A. Veneziani. Hierarchical model reduction for incompressible fluids in pipes. *Internat. J. Numer. Methods Engrg.*, 114(5):469–500, 2018.
- [16] Bernd Heinrich. The Fourier-finite-element method for Poisson’s equation in axisymmetric domains with edges. *SIAM J. Numer. Anal.*, 33(5):1885–1911, 1996.
- [17] J.S. Hesthaven, G. Rozza, and B. Stamm. *Certified Reduced Basis Methods for Parametrized Partial Differential Equations*. SpringerBriefs in Mathematics. Springer, Cham; BCAM Basque Center for Applied Mathematics, Bilbao, 2016.

- [18] M. Hinze and M. Kunkel. Residual based sampling in POD model order reduction of drift-diffusion equations in parametrized electrical networks. *ZAMM Z. Angew. Math. Mech.*, 92(2):91–104, 2012.
- [19] M. Kahlbacher and S. Volkwein. Galerkin proper orthogonal decomposition methods for parameter dependent elliptic systems. *Discuss. Math. Differ. Incl. Control Optim.*, 27(1):95–117, 2007.
- [20] G. Kerschen, J. Golinval, A.F. Vakakis, and L.A. Bergman. The method of Proper Orthogonal Decomposition for dynamical characterization and order reduction of mechanical systems: an overview. *Nonlinear Dynam.*, 41(1-3):147–169, 2005.
- [21] K. Kunisch and S. Volkwein. Galerkin proper orthogonal decomposition methods for parabolic problems. *Numer. Math.*, 148:117–148, 2001.
- [22] K. Kunisch and S. Volkwein. Galerkin proper orthogonal decomposition methods for a general equation in fluid dynamics. *SIAM J. Numer. Anal.*, 40(2):492–515, 2002.
- [23] L. Mansilla Alvarez, P. Blanco, C. Bulant, E. Dari, A. Veneziani, and R. Feijóo. Transversally enriched pipe element method (TEPEM): an effective numerical approach for blood flow modeling. *Int. J. Numer. Methods Biomed. Eng.*, 34(4):e02808, 2017.
- [24] M. Ohlberger and K. Smetana. Approximation of skewed interfaces with tensor-based model reduction procedures: application to the reduced basis hierarchical model reduction approach. *J. Comput. Phys.*, 321:1185–1205, 2016.
- [25] S. Perotto. Hierarchical model (Hi-Mod) reduction in non-rectilinear domains. In *Domain Decomposition Methods in Science and Engineering XXI*, volume 98 of *Lect. Notes Comput. Sci. Eng.*, pages 477–485. Springer, Cham, 2014.
- [26] S. Perotto. A survey of hierarchical model (Hi-Mod) reduction methods for elliptic problems. In S.R. Idelsohn, editor, *Numerical Simulations of Coupled Problems in Engineering*, volume 33 of *Comput. Methods Appl. Sci.*, pages 217–241. Springer, Cham, 2014.
- [27] S. Perotto, M.G. Carlino, and F. Ballarin. Model reduction by separation of variables: a comparison between Hierarchical Model reduction and Proper Generalized Decomposition. In S.J. Sherwin, D. Moxey, J. Peiró, P.E. Vincent, and C. Schwab, editors, *Spectral and High Order Methods for Partial Differential Equations. ICOSAHOM 2018*, volume 134 of *Lect. Notes Comput. Sci. Eng.* Springer Nature Switzerland, 2020. To appear.
- [28] S. Perotto, A. Ern, and A. Veneziani. Hierarchical local model reduction for elliptic problems: a domain decomposition approach. *Multiscale Model. Simul.*, 8(4):1102–1127, 2010.

- [29] S. Perotto, A. Reali, P. Rusconi, and A. Veneziani. HIGAMod: a hierarchical isogeometric approach for model reduction in curved pipes. *Comput. & Fluids*, 142:21–29, 2017.
- [30] S. Perotto and A. Veneziani. Coupled model and grid adaptivity in hierarchical reduction of elliptic problems. *J. Sci. Comput.*, 60(3):505–536, 2014.
- [31] S. Perotto and A. Zilio. Hierarchical model reduction: three different approaches. In A. Cangiani, R.L. Davidchack, E. Georgoulis, A.N. Gorban, J. Levesley, and Tretyakov M.V., editors, *Numerical Mathematics and Advanced Applications*, pages 851–859. Springer-Verlag Berlin Heidelberg, 2013.
- [32] S. Perotto and A. Zilio. Space-time adaptive hierarchical model reduction for parabolic equations. *Adv. Model. and Simul. in Eng. Sci.*, 2:25, 2015.
- [33] A. Quarteroni, A. Manzoni, and F. Negri. *Reduced Basis Methods for Partial Differential Equations*, volume 92 of *Unitext*. Springer, Cham, 2016.
- [34] M. Vogelius and I. Babuška. On a dimensional reduction method. I. The optimal selection of basis functions. *Math. Comp.*, 37(155):31–46, 1981.
- [35] S. Volkwein. Optimality system POD and a-posteriori error analysis for linear-quadratic problems. *Control. Cybern.*, 291:1109–1125, 2011.
- [36] S. Volkwein. Proper Orthogonal Decomposition: Theory and Reduced-Order Modelling. Lecture notes, University of Konstanz, 2013.
- [37] S. Walton, O. Hassan, and K. Morgan. Reduced order modelling for unsteady fluid flow using proper orthogonal decomposition and radial basis functions. *Appl. Math. Model.*, 37(20-21):8930–8945, 2013.
- [38] H. Wendland. Piecewise polynomial, positive definite and compactly supported radial functions of minimal degree. *Adv. Comput. Math.*, 4(4):389–396, 1995.
- [39] M. Zancanaro, F. Ballarin, S. Perotto, and G. Rozza. Hierarchical model reduction techniques for flow modeling in a parametrized setting. MOX-report 35/2019, Politecnico di Milano, 2019.

MOX Technical Reports, last issues

Dipartimento di Matematica
Politecnico di Milano, Via Bonardi 9 - 20133 Milano (Italy)

- 55/2020** Botti, M.; Castanon Quiroz, D.; Di Pietro, D.A.; Harnist, A.
A Hybrid High-Order method for creeping flows of non-Newtonian fluids
- 56/2020** Botti, L.; Botti, M.; Di Pietro, D. A.;
A Hybrid High-Order method for multiple-network poroelasticity
- 57/2020** Regazzoni, F.; Quarteroni, A.
An oscillation-free fully partitioned scheme for the numerical modeling of cardiac active mechanics
- 58/2020** Beraha, M.; Pegoraro, M.; Peli, R.; Guglielmi, A
Spatially dependent mixture models via the Logistic Multivariate CAR prior
- 59/2020** Massi, M.C.; Franco, N.R; Ieva, F.; Manzoni, A.; Paganoni, A.M.; Zunino, P.
High-Order Interaction Learning via Targeted Pattern Search
- 54/2020** Arnone, E.; Bernardi, M. S.; Sangalli, L. M.; Secchi, P.
Analysis of Telecom Italia mobile phone data by space-time regression with differential regularization
- 53/2020** Arnone, E.; Kneip, A.; Nobile, F.; Sangalli, L. M.
Some numerical test on the convergence rates of regression with differential regularization
- 52/2020** Arnone, E.; Kneip, A.; Nobile, F.; Sangalli, L. M.
Some first results on the consistency of spatial regression with partial differential equation regularization
- 51/2020** Ferraccioli, F.; Sangalli, L. M.; Arnone, E.; Finos, L.
A functional data analysis approach to the estimation of densities over complex regions
- 50/2020** Bonaventura, L.; Gomez Marmol, M.
The TR-BDF2 method for second order problems in structural mechanics